Photodetachment of Multiply Charged Anions: The Electronic Structure of Gaseous Square-Planar Transition Metal Complexes PtX_4^{2-} (X = Cl, Br)

Xue-Bin Wang and Lai-Sheng Wang*

Contribution from the Department of Physics, Washington State University, 2710 University Drive, Richland, Washington 99352, and W. R. Wiley Environmental Molecular Sciences Laboratory, MS K8-88, Pacific Northwest National Laboratory, P.O. Box 999, Richland, Washington 99352

Received September 29, 1999

Abstract: Two square-planar 5d transition metal complexes, PtX_4^{2-} (X = Cl, Br), were observed in the gas phase using ion-trap mass spectrometry and an electrospray ionization source. Photodetachment photoelectron spectroscopy was used to probe their electronic structure, and their photoelectron spectra were measured at three photon energies, 193, 266, and 355 nm. The spectra for the two complexes were found to be similar, each with 10 well-resolved electronic features. These observed detachment features were qualitatively interpreted using the currently available theoretical calculations. The unprecedented resolution of the spectra afforded in the gas phase allowed us to definitely determine the ground state molecular energy levels for these classical square-planar metal complexes. We found that in $PtCl_4^{2-}$ all the d-orbitals are above the ligand-derived orbitals, whereas in $PtBr_4^{2-}$ all the d-orbitals are stabilized while the ligand-orbitals are destabilized, leading to an overlap between the d- and ligand-orbitals. Furthermore, the binding energies of the second excess electron in PtX_4^{2-} were found surprisingly to be negative by −0.25 and −0.04 eV for X = Cl and Br, respectively. The negative electron-binding energies indicate that the two gaseous dianions are in fact electronically unstable against electron loss owing to the strong intramolecular Coulomb repulsion between the two excess charges. Photon-energy-dependent studies clearly revealed the dianion nature of these species and allowed the repulsive Coulomb barriers to be estimated.

Introduction

Square-planar PtX_4^{2-} species (X = Cl, Br) are classical Werner-type transition metal complexes and are commonly found in solutions and solids.[1,2] They are involved in a number of catalytic chemical reactions and have been studied extensively both experimentally[3−11] and theoretically.[12−18] However, the electronic structure of the square-planar transition metal complexes remains a topic of continuing interest and controversy because of a lack of decisive experimental data. The controversy centers mainly on the order of the molecular orbital energy levels and the degree of covalency in the metal−ligand bonds. All previous spectroscopic information on the PtX_4^{2-} species was obtained from the condensed phases whereas the theoretical calculations tended to be done on isolated molecular species. The intrinsic low resolution and the effects of the condensed phase environments left many ambiguities in terms of the assignments of the energy levels of these complexes. Up until now, gaseous PtX_4^{2-} species have never been observed and there is no gas-phase experimental information available on these important inorganic metal complexes.

Gas-phase studies of these species would be much desirable and the obtained molecular and spectroscopic information can be used to compare directly to theoretical calculations, which are often done on gaseous species. Furthermore, from the point of view of multiply charged anions, it would be interesting to know if the pentaatomic species can be made in the gas phase and to learn about their stability and intramolecular Coulomb repulsion.

Recently we have developed an experimental technique to investigate gas-phase multiply charged anions (MCA's) using photodetachment photoelectron spectroscopy (PES) and an electrospray ionization source coupled with ion-trap mass spectrometry.[19] We have observed many multiply charged

* Address correspondence to this author at Washington State University.

(1) Bray, M. R.; Deeth, R. J.; Paget, V. J.; Sheen, P. D. *Int. J. Quantum Chem.* **1996**, *61*, 85.
(2) Cotton, F. A.; Wilkinson, G. *Advanced Inorganic Chemistry*; Wiley: New York, 1988.
(3) Caminiti, R.; Carbone, M.; Sadun, C. J. *Mol. Liq.* **1998**, *75*, 149.
(4) Waltz, W. L.; Lilie, J.; Goursot, A.; Chermette, H. *Inorg. Chem.* **1989**, *28*, 2247.
(5) Chatt, J.; Gamlen, G. A.; Orgel, L. E. *J. Chem. Soc.* **1958**, 486.
(6) Anex, B. G.; Takeuchi, N. *J. Am. Chem. Soc.* **1974**, *96*, 4411.
(7) Elding, L. I.; Olsson, L. F. *J. Phys. Chem.* **1978**, *82*, 69 and references therein.
(8) Martin, D. S., Jr.; Foss, J. G.; McCarville, M. E.; Tucker, M. A.; Kassman, A. J. *Inorg. Chem.* **1966**, *5*, 491.
(9) Piepho, S. B.; Schatz, P. N.; McCaffery, A. J. *J. Am. Chem. Soc.* **1969**, *91*, 5994.
(10) Biloen, P.; Prins, R. *Chem. Phys. Lett.* **1972**, *16*, 611.
(11) Moddeman, W. E.; Blackburn, J. R.; Kumar, G.; Morgan, K. A.; Albridge, R. G.; Jones, M. M. *Inorg. Chem.* **1972**, *11*, 1715.
(12) Fenske, R. F.; Martin, D. S., Jr.; Ruedenberg, K. *Inorg. Chem.* **1962**, *1*, 441.
(13) Gray, H. B.; Ballhausen, C. J. *J. Am. Chem. Soc.* **1963**, *85*, 260.
(14) Cotton, F. A.; Harris, C. B. *Inorg. Chem.* **1967**, *6*, 369.
(15) Basch, H.; Gray, H. B. *Inorg. Chem.* **1967**, *6*, 365.
(16) Messmer, R. P.; Interrante, L. V.; Johnson, K. H. *J. Am. Chem. Soc.* **1974**, *96*, 3847.
(17) Messmer, R. P.; Wahlgren, U.; Johnson, K. H. *Chem, Phys. Lett.* **1973**, *18*, 7.
(18) Larsson, S.; Olsson, L.-F.; Rosen, A. *Int. J. Quantum Chem.* **1984**, *25*, 201.
(19) Wang, L. S.; Ding, C. F.; Wang, X. B.; Barlow, S. E. *Rev. Sci. Instrum.* **1999**, *70*, 1957.

10.1021/ja9935106 CCC: $19.00
Published on Web 02/26/2000

anions in the gas phase and discovered a number of interesting phenomena about gaseous MCA's. We have demonstrated that PES is a particularly ideal experimental technique to probe the intrinsic properties of free MCA's. For example, we have directly observed the repulsive Coulomb barrier (RCB),[20] created by a long-range Coulomb repulsion and a short-range electron binding, that is universally present in any gaseous MCA.[21−23] We have determined the relationship between the magnitude of the RCB and the intramolecular Coulomb repulsion.[24] In particular, we have shown that the RCB can prevent electron detachment even when the photon energies are higher than the electron binding energies.[20,24−29] In addition to giving information about the electronic stability, PES is capable of yielding direct electronic structure information about the MCA's, as we have shown very recently for a series of free hexahalogenometalate doubly charged anions, $[ML_6]^{2-}$ (M = Re, Os, Ir, Pt; L = Cl and Br).[30] It is thus natural for us to search for the gaseous pentaatomic metal complexes and obtain information about their electronic structure. However, these relatively small systems post considerable experimental challenges because of their instability, understandably caused by the strong intramolecular Coulomb repulsion. Our extensive effort to search for the smallest stable gaseous MCA's and our in-depth discussions about the electronic and thermodynamic stability of small MCA's can be found in a very recent publication.[31]

In this paper, we present the details of the PES spectra of the two square-planar transition metal complexes, $PtCl_4^{2-}$ and $PtBr_4^{2-}$, that we were able to observe in the gas phase. We obtained the PES spectra of the two species at three photon energies: 355 (3.496 eV), 266 (4.661 eV), and 193 nm (6.424 eV). We show that these two late 5d transition metal tetrahalide complexes are in fact unstable against electron autodetachment, but they have sufficient lifetimes to allow their PES spectra to be measured. We found the second electron binding energies of $PtCl_4^{2-}$ and $PtBr_4^{2-}$ to be negative by −0.25 and −0.04 eV, respectively. The observability of these dianions in the gas phase is due to the RCB that prevents the "negatively bound" electron from immediate autodetachment. More interestingly, well-resolved detachment features were obtained in the PES spectra, yielding a wealth of electronic structure information about both the dianions and the singly charged anions. Detachments from the central metal d-orbitals and ligand p-orbitals were clearly observed and distinguished, and are qualitatively explained based on previous theoretical calculations. We found that the electronic structures of the Cl- and Br-complexes are qualitatively the same, but with slightly different relative orderings between their metal-d and ligand-p orbitals. The current results provide unprecedented and well-resolved electronic structure information about these two classical metal complexes and can be used quantitatively to verify more accurate quantum mechanical calculations where the relativistic effects are expected to play a major role.

Experimental Section

The experimental apparatus consists of a magnetic-bottle time-of-flight PES apparatus coupled to an electrospray ion source and an ion-trap time-of-flight mass spectrometer. Details of the apparatus have been described elsewhere.[19] The electrospray solution contained 10^{-3} M K_2PtX_4 (X = Cl or Br) desolved in a water/methanol (10/90) mixed solvent at neutral pH. The solution was sprayed through a 20-μm-diameter quartz capillary at ambient conditions and a high-voltage bias of −2.2 kV. The liquid droplets from the electrospray capillary were fed into a 0.8-mm-diameter stainless steel desolvation capillary, which was heated to ∼70 °C. The anions that emerged from the desolvation capillary were guided by a radio frequency quadrupole ion-guide into a quadrupole ion-trap, where the ions were accumulated and trapped for 0.1 s before being pushed out and analyzed by the time-of-flight mass spectrometer. There are three main anion species, X^-, PtX_3^-, and PtX_4^{2-}. The PtX_4^{2-} signals were very weak due to the extensive solvolysis in water solution[2] and the metastable nature in the gas phase for these species (discussed later), especially for the chloride complex. The PtX_3^- signals had about the same abundance as those of the PtX_4^{2-} dianions, whereas the atomic anions X^- were about 10 times stronger than either of the molecular anions. Furthermore, we found that our dianion signals were only stable for about half an hour after we started the electrospray and then the desolvation capillary had to be cleaned or changed. We suspected that the PtX_4^{2-} dianions were consumed in the desolvation capillary through catalytic reactions due to the accumulation of Pt-containing deposit on the inner walls of the desolvation capillary.

The dianions of interest were mass-selected in the time-of-flight mass spectrometer and decelerated before being intercepted by a probe laser beam in the photodetachment zone of the magnetic-bottle photoelectron analyzer. We used both an ArF excimer laser (193 nm) and a Q-switched Nd:YAG laser (355 and 266 nm) for photodetachment. The PES experiments were performed at 20 Hz with the ion beam off at alternating laser shots for background subtraction. Photoelectrons were collected at nearly 100% efficiency by the magnetic-bottle and analyzed in a 4-m electron flight tube. The measured electron time-of-flight distributions were converted to kinetic energy (KE) spectra calibrated using the known spectra of I^- and O^-. The electron binding energies (BE) were determined from the Einstein's photoelectric equation, $h\nu$ = BE + KE. The electron kinetic energy resolution was $\Delta KE/KE \sim 2\%$, i.e., 20 meV for 1 eV kinetic-energy electrons. Because of the instability of the electrospray source during the experiments, photoelectron spectra could only be accumulated for about half an hour. Several runs had to be taken and then added together to obtain better statistics, which in turn deteriorated the resolution to some degree.

We can trap ions in our ion-trap for up to 400 s. Thus, lifetimes can be estimated for metastable multiply charged species with lifetimes <400 s. In such experiments, we used a mechanical chopper to load the ion-trap for a predetermined period of time (usually ∼0.1 s). The trapping time was then varied systematically while the ion intensity was monitored with the time-of-flight mass spectrometer. The trapping efficiency of the ion-trap itself was calibrated using stable molecular ions.

Results

$PtCl_4^{2-}$. Figure 1 shows the PES spectra of $PtCl_4^{2-}$ at three detachment photon energies. The 193-nm spectrum (Figure 1a) exhibits rich and well-resolved features, as labeled by the letters X and A−I. The 266- and 355-nm spectra resolved the X and A, C and D features very clearly compared to the 193-nm spectrum, where the X and A features were not resolved and the D feature was shown only as a shoulder. Noticeably, the G, H, and I features disappeared in the 266-nm spectra (Figure 1b). The E and F features almost disappeared in the 355-nm spectra where the C and D features also showed significantly reduced relative intensities.

(20) Wang, X. B.; Ding, C. F.; Wang, L. S. *Phys. Rev. Lett.* **1998**, *81*, 3551.
(21) Scheller, M. K.; Compton, R. N.; Cederbaum, L. S. *Science* **1995**, 270, 116.
(22) Boldyrev, A. I.; Gutowski, M.; Simons, J. *Acc. Chem. Res.* **1996**, *29*, 497.
(23) Yannouleas, C.; Landman, U. *Chem. Phys. Lett.* **1993**, *210*, 437.
(24) Wang, L. S.; Ding, C. F.; Wang, X. B.; Nicholas, J. B. *Phys. Rev. Lett.* **1998**, *81*, 2667.
(25) Ding, C. F.; Wang, X. B.; Wang, L. S. *J. Phys. Chem. A* **1998**, *102*, 8633.
(26) Ding, C. F.; Wang, X. B.; Wang, L. S. *J. Chem. Phys.* **1999**, *110*, 3635.
(27) Wang, X. B.; Ding, C. F.; Nicholas, J. B.; Dixon, D. A.; Wang, L. S. *J. Phys. Chem. A* **1999**, *103*, 3423.
(28) Wang, X. B.; Ding, C. F.; Wang, L. S. *Chem. Phys. Lett.* **1999**, *307*, 391.
(29) Wang, X. B.; Wang, L. S. *Nature* **1999**, *400*, 245.
(30) Wang, X. B.; Wang, L. S. *J. Chem. Phys.* **1999**, *111*, 4497.
(31) Wang, X. B.; Wang, L. S. *Phys. Rev. Lett.* **1999**, *83*, 3402.

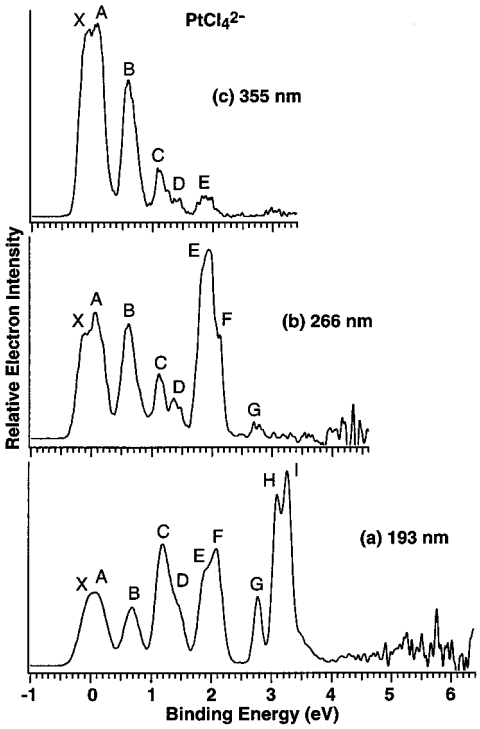

Figure 1. Photoelectron spectra of $PtCl_4^{2-}$ at (a) 193 (6.424 eV), (b) 266 (4.661 eV), and (c) 355 nm (3.496 eV). Note the negative binding energy feature (X) revealed at all three different detachment photon energies. The letters label the resolved electronic features.

The photon-energy-dependent spectral features shown here were caused by the RCB, vividly revealing the dianion nature of $PtCl_4^{2-}$. The magnitude of the RCB can be estimated based on these data, as discussed later. The relative intensities of the X, A, and B features were unchanged from 193 to 266 nm. However, the relative intensities of the C and D features were reduced at 266 nm whereas that of the E feature was considerably enhanced at 266 nm, compared to the 193-nm spectrum. The intensity changes of the C, D, and E features from 193 to 266 nm are due to the nature of the detachment channels, and are not related to the RCB.

The most surprising observation in the PES spectra of $PtCl_4^{2-}$ is the fact that the X feature has a negative binding energy. The adiabatic detachment energy was measured to be −0.25 (0.05) eV, obtained by drawing a straight line at the leading edge of the 355-nm spectrum and then adding a constant of 0.07 eV to take into account the resolution. The adiabatic binding energy of the A feature was also negative, but could not be directly measured because of the overlap with the X feature. The electron kinetic energy scales were carefully calibrated before and after each PES experiment and different photon fluxes were employed to rule out any multiphoton processes. Thus the negative electron binding energies of $PtCl_4^{2-}$ were firmly established. The vertical detachment energy of the X feature was measured to be −0.10 eV and that of the A feature was 0.10 eV. The vertical binding energies of all the observed spectral features are given in Table 1.

The negative binding energy observed for $PtCl_4^{2-}$ is interesting and suggests that this pentaatomic dianion is in fact electronically unstable, or metastable considering its seemingly long lifetime. To confirm the metastability of $PtCl_4^{2-}$, we further measured its lifetime using our ion-trap by measuring relative ion intensities at different trapping times. The estimated half-life of the $PtCl_4^{2-}$ dianion was approximately ∼0.2 s. This half-life has been confirmed in our previous study by performing electron-tunneling calculations with a simple model Coulomb barrier.[31]

Table 1. Vertical Detachment Energies (VDE in eV)[a] of All the Detachment Features Observed in the PES Spectra of PtX_4^{2-} (X = Cl, Br)[b]

	X	A	B	C	D	E	F	G	H	I
$PtCl_4^{2-}$										
VDE	−0.10	0.10	0.65	1.15	1.40	1.90	2.08	2.78	3.10	3.26
ΔE	0.00	0.20	0.75	1.29	1.50	2.00	2.18	2.88	3.20	3.36
$PtBr_4^{2-}$										
VDE	0.11	0.33	0.87	1.04	1.31	1.49	1.84	2.61	2.92	3.10
ΔE	0.00	0.22	0.76	0.93	1.20	1.38	1.73	2.50	2.81	2.99

[a] The uncertainties for the VDE's are ±0.05 eV. [b] ΔE − VDE relative to the X ground state. All labels are referred to Figures 1 and 2.

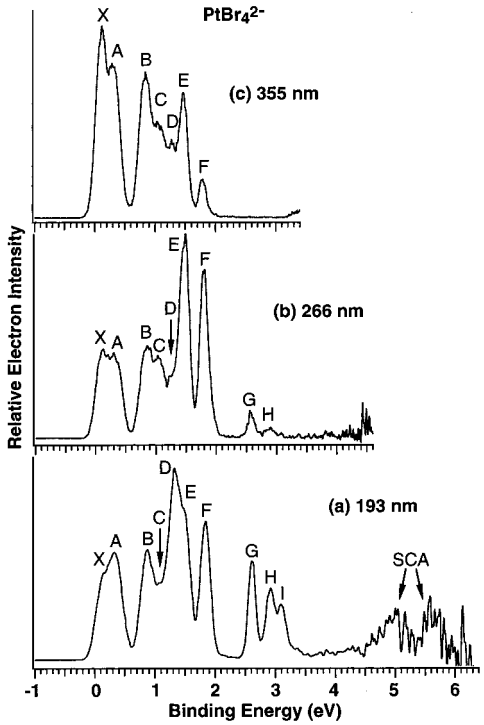

Figure 2. Photoelectron spectra of $PtBr_4^{2-}$ at (a) 193, (b) 266, and (c) 355 nm. Note the one-to-one correspondence between the features of $PtBr_4^{2-}$ and $PtCl_4^{2-}$. The X feature of $PtBr_4^{2-}$ also shows a slightly negative binding energy. "SCA" indicates signals from singly charged anion, $PtBr_4^-$, formed from detachment of the dianion.

$PtBr_4^{2-}$. To compare to the spectra of $PtCl_4^{2-}$ and understand the nature of all the observed detachment transitions, we also measured the PES spectra of $PtBr_4^{2-}$, as shown in Figure 2. Again, well-resolved spectral features were observed and labeled with the letters X and A−I. In general, the spectral features of $PtBr_4^{2-}$ are quite similar to that of $PtCl_4^{2-}$, as expected. Similar photon-energy dependence was observed, with high binding energy features disappearing in the lower photon energy spectra. In fact, there exists a one-to-one correspondence between the features of the $PtBr_4^{2-}$ and $PtCl_4^{2-}$ spectra, with some variations of spectral intensities at different photon energies. The first feature (X) revealed a slightly negative binding energy of −0.04 (0.05) eV, indicating that $PtBr_4^{2-}$ is also electronically unstable relative to an electron loss. However, we see that the bromide complex is electronically more stable than the chloride complex by 0.21 eV, despite the fact that the Cl atom has a higher

electron affinity than the Br atom. The vertical binding energies of all the observed detachment features of $PtBr_4^{2-}$ are also given in Table 1.

The successive disappearance of the high binding energy features in the lower photon energy spectra (266 and 355 nm) was similar to that in the $PtCl_4^{2-}$ spectra (Figure 1), again a direct consequence of the RCB in $PtBr_4^{2-}$. The relative intensity of the X feature appeared to be increasing as the photon energy decreased. The most striking change of spectral intensity with the photon energy comes from the D feature, which is dominant in the 193-nm spectrum, but becomes very weak in both the 266- and 355-nm spectra. The photon-energy dependence of the D feature in $PtBr_4^{2-}$ is similar to that of the C feature in $PtCl_4^{2-}$ (Figure 1). The very broad features, labeled "SCA" in the 193-nm spectrum of $PtBr_4^{2-}$, were due to detachment of the corresponding singly charged anion, $PtBr_4^-$, by the absorption of a second photon following the photodetachment of the dianion. Similar signals also existed in the 193-nm spectrum of $PtCl_4^{2-}$ (Figure 1a), but with much lower intensities.

We also estimated the half-life of $PtBr_4^{2-}$ to be ~60 s using the ion-trap. Our previous tunneling calculations indicated that $PtBr_4^{2-}$ should have a much longer electron-tunneling lifetime than the measured value.[31] The long calculated electron-tunneling lifetime was due to the fact that the binding energy of $PtBr_4^{2-}$ was barely negative (−0.04 eV) and the long tail of the RCB. Therefore, the observed relatively short lifetime of $PtBr_4^{2-}$ is probably due to fragmentation. Although there have been no theoretical studies on $PtBr_4^{2-}$, it is likely to be thermodynamically unstable against the fragmentation channel: $PtBr_4^{2-} \rightarrow PtBr_3^- + Br^-$, due to the strong Coulomb repulsion. It may be important to point out that many small metal halide dianions have been predicted to be thermodynamically unstable (against fragmentation) despite the fact that they are electronically stable (against electron detachment).[32−40] Because a potential barrier, similar to the RCB for electron detachment, exists for such charge separation fragmentation, very long lifetimes have been predicted for these dianions. Interestingly, a recent theoretical study[41] on the lifetime of LiF_3^{2-} suggested that temperature plays a very important role in determining the lifetime of such metastable MCA's. Although LiF_3^{2-} is predicted to have a lifetime of 10^{17} s below 20 K, it drops down to $<10^{-5}$ s above 80 K. The trapping mechanism of our ion-trap involves collisions with background gas under the influence of the RF field, resulting in relatively high temperatures for the trapped ions (room temperature or slightly above).[42] We concluded that the relatively short lifetime of $PtBr_4^{2-}$ was primarily due to its thermodynamic metastability against fragmentation, i.e., $PtBr_4^{2-} \rightarrow PtBr_3^- + Br^-$, plus the relatively high-temperature conditions of the ion-trap. We have direct evidence for this decay channel. During the lifetime measurements, we observed that as the $PtBr_4^{2-}$ signal decreases the $PtBr_3^-$ signal increases accordingly.

Table 2. Measured Adiabatic Electron Binding Energies (ADE, eV), Estimated Repulsive Coulomb Barriers (RCB, eV), and Measured Half-Lives (s) for PtX_4^{2-} (X = Cl and Br)

	$PtCl_4^{2-}$	$PtBr_4^{2-}$
ADE	−0.25 (0.05)	−0.04 (0.05)
RCB	~2.5	~2.1
half-life	~0.2	~60

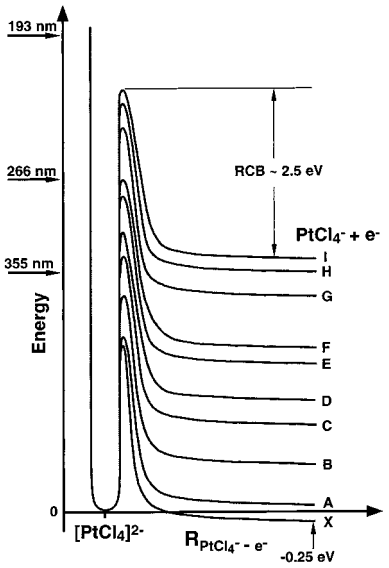

Figure 3. Schematic drawing of potential energy curves showing the repulsive Coulomb barriers (RCB) of $PtCl_4^{2-}$ with respect to the different asymptotic states (X to I) of the corresponding singly charged anion, $PtCl_4^-$. The estimated RCB for $PtCl_4^{2-}$ in eV and the relative positions of the three photon energies used are also indicated.

The adiabatic binding energies, i.e., the adiabatic electron affinities of the corresponding monoanions and the measured half-lives, are given in Table 2. The detailed spectral assignments are discussed next.

Discussion

Photon-Energy-Dependent PES Features and the Repulsive Coulomb Barriers in MCA's. Before discussing the details of the PES spectra of $PtCl_4^{2-}$ and $PtBr_4^{2-}$, we first consider the photon-energy-dependent PES spectra and explain the successive disappearance of the high binding-energy features in the lower photon energy spectra. As we reported previously,[24−31] there is an essential difference between photodetachment of multiply and singly charged anions. There exists a RCB against electron detachment in MCA's, due to the long-range Coulomb repulsion between the outgoing electron and the remaining anion (which has one less charge than the parent MCA). Figure 3 schematically illustrates the RCB's of the $PtCl_4^{2-}$ dianion relating to the different asymptotic electronic states (X to I) of the singly charged anion, $PtCl_4^-$, as well as the relative positions of the different detachment photon energies. The barrier height is measured from the top of a potential curve relative to an asymptotic limit of the singly charged anionic states. The well depths are different leading to the different asymptotic electronic states of the singly charged anion, simply because these states have different electron binding energies. When a detachment photon energy is lower than the well depth for a given state, there will not be direct photodetachment signals leading to this state (except through

(32) Weikert, H. G.; Cederbaum, L. S.; Tarantelli, F.; Boldyrev, A. I. *Z. Phys. D* **1991**, *18*, 2999.
(33) Scheller, M. K.; Cederbaum, L. S. *J. Chem. Phys.* **1993**, *99*, 441.
(34) Weikert, H. G.; Cederbaum, L. S. *J. Chem. Phys.* **1993**, *99*, 8877.
(35) Scheller, M. K.; Cederbaum, L. S. *Chem. Phys. Lett.* **1993**, *216*, 141.
(36) Scheller, M. K.; Cederbaum, L. S. *J. Chem. Phys.* **1994**, *100*, 8934, 8943. Scheller, M. K.; Cederbaum, L. S. *J. Chem. Phys.* **1994**, *101*, 3962.
(37) Boldyrev, A. I.; Simons, J. *J. Chem. Phys.* **1992**, *97*, 2826.
(38) Boldyrev, A. I.; Simons, J. *J. Chem. Phys.* **1993**, *98*, 4745.
(39) Gutowski, M.; Boldyrev, A. I.; Ortiz, J. V.; Simons, J. *J. Am. Chem. Soc.* **1994**, *116*, 9262.
(40) Gutowski, M.; Boldyrev, A. I.; Simons, J.; Rak, J.; Blazejowski, J. *J. Am. Chem. Soc.* **1996**, *118*, 1173.
(41) Sommerfeld, T.; Child, M. S. *J. Chem. Phys.* **1999**, *110*, 5670.
(42) March, R. E.; Todd, J. F. J. *Practical Aspects of Ion Trap Mass Spectrometry*; CRC Press: New York, 1995; Vols. I−III.

electron tunneling[28]), even if the photon energy is higher than the binding energy of this state. When the photon energy is near the top of a specific potential curve, the photoelectron signals corresponding to this state will be reduced, i.e., the detachment cross section will be reduced due to either tunneling or barrier reflection.

In the PES spectra of $PtCl_4^{2-}$ (Figure 1), 10 distinct electronic features were observed, as labeled from X to I, corresponding to the ground and nine excited states of $PtCl_4^-$. If we assume that the RCB height is the same for all the detachment channels, we can estimate it from the photon-energy-dependent PES spectra. The disappearance of the G, H, and I features in the 266-nm spectrum indicated that the 266-nm photon energy (4.661 eV) lies below the top of the potential curves of these states (see Figure 3). Thus the RCB has to be larger than 1.88 eV ($h\nu$ − BE of the G state). The strong E-feature (BE = 1.90 eV) in the 266-nm spectrum implies that the photon energy is above the RCB of the E state. Thus the RCB must be smaller than 2.76 eV (4.66−1.90 eV). Therefore we can bracket the RCB as 1.88 eV < RCB < 2.76 eV. The intensity of the F-feature (BE = 2.08 eV) in the 266-nm spectrum was significantly reduced, indicating that the photon energy is probably around the top of the barrier corresponding to the F detachment channel. Thus we deduced a barrier height of ∼2.5 eV for the $PtCl_4^{2-}$ dianion (4.66−2.08 eV). Therefore, the photoelectron signals corresponding to the C, D, and E features in the 355-nm spectrum were due to electron tunneling since the 355-nm photon was below their RCB (Figure 3). Their reduced intensities in the 355-nm spectra were consistent with the tunneling mechanism, and indirectly validating the derived RCB height.

We can also estimate the RCB for $PtBr_4^{2-}$ from its photon-energy-dependent PES spectra (Figure 2). The weak signal of the G feature (BE = 2.61 eV) and the strong intensity of the F feature (BE = 1.84 eV) in the 266-nm PES spectrum indicated that the 266-nm photon is above the barrier of the F state, but below that of the G state. Thus we deduced that the RCB for $PtBr_4^{2-}$ should be between 2.05 (4.66−2.61 eV) and 2.82 eV (4.66−1.84 eV). The very weak signal of the F feature and the reduced relative intensity of the E feature (BE = 1.49 eV) in the 355-nm spectrum suggest that the 355-nm photon was near the barrier top of the E state. We thus deduced a RCB for $PtBr_4^{2-}$ to be about 2.1 eV.

As we reported previously,[24] the RCB in MCA's is equal in magnitude to the intramolecular Coulomb repulsion. The smaller RCB in $PtBr_4^{2-}$ than in $PtCl_4^{2-}$ is consistent with the slightly larger size in the former, thus giving rise to a smaller intramolecular Coulomb repulsion. This also explains why $PtBr_4^{2-}$ is electronically more stable than $PtCl_4^{2-}$ by 0.2 eV despite the fact that Cl has a higher electron affinity (3.613 eV) than that of Br (3.365 eV).[43] This clearly demonstrates the dominant role of intramolecular Coulomb repulsion in determining the stability of MCA's in the gas phase. There have been significant recent theoretical efforts trying to understand the properties of gaseous MCA's.[21,22,32−41,44] It is also interesting to point out the Coulomb repulsion also exists in multiply charged cations[45] and has been observed in proton affinity experiments.[44−47]

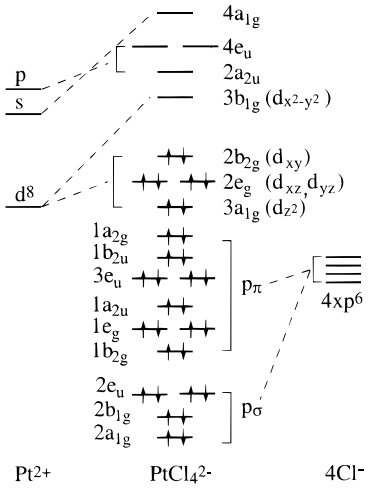

Figure 4. Molecular orbital diagram for the square-planar $PtCl_4^{2-}$ metal complex (**15**).

The unusual phenomena of a negative electron binding energy can only occur in MCA's due to the RCB, which provides dynamic stability and prevents the unbound electron from immediate autodetachment. C_{60}^{2-} is probably the first electronically metastable dianions observed,[48,49] although its second electron binding energy is still not known experimentally.[21] Our previous effort to produce this metastable dianion using electrospray was not successful.[50] The current results constitute only the second direct measurement of negative electron binding energies in MCA's; we have recently reported a much larger negative binding energy in a quadruply charged anion.[29] In another recent study,[31] we confirmed, using electron tunneling calculations through a model Coulomb potential, that the short lifetime of the $PtCl_4^{2-}$ dianion was indeed determined by its negative electron binding energy against electron tunneling. On the other hand, the lifetime of $PtBr_4^{2-}$ was not limited by its electronic instability, but rather by its thermodynamic instability against fragmentation, i.e., $PtBr_4^{2-}$ is not thermodynamically stable relative to $PtBr_3^- + Br^-$. From the estimated 2.1 eV intramolecular Coulomb repulsion in $PtBr_4^{2-}$, we can further conclude that the $Br_3Pt^- - Br^-$ bond energy should be smaller than 2.1 eV.

Molecular Orbitals of $PtCl_4^{2-}$ and Assignments of the PES Features. The PES features shown in Figures 1 and 2 represent transitions from the ground state of the dianions to the ground and excited states of the corresponding singly charged anions. Within the single-particle approximation (Koopmans' theorem), these PES features can be alternatively viewed as removing electrons from the occupied molecular orbitals (MO's) of the dianions. $PtCl_4^{2-}$ is a planar square molecule with a d^8 configuration. Under the D_{4h} symmetry, the five d-orbitals of Pt are split to four sets: $d_{x^2-y^2}$ ($3b_{1g}$), d_{xy} ($2b_{2g}$), d_{xz} and d_{yz} ($2e_g$), and d_{z^2} ($3a_{1g}$). It is known that for $PtCl_4^{2-}$, the relatively high ligand-field strength makes it inherently adopt the low-spin arrangement.[18] Therefore the ground state of $PtCl_4^{2-}$ is a closed-shell species with one empty d-orbital. Many early MO studies have been carried out on $PtCl_4^{2-}$ to interpret the observed absorption bands in solutions.[12−18] Figure 4 shows an MO diagram of $PtCl_4^{2-}$ according to Basch and Gray.[15]

(43) Hotop, H.; Lineberger, W. C. *J. Phys. Chem. Ref. Data* **1985**, *14*, 731.
(44) Gronert, S. *Int. J. Mass Spetrom.* **1999**, *185*, 351.
(45) For a recent review, see: Schroder, D.; Schwarz, H. *J. Phys. Chem. A* **1999**, *103*, 7385.
(46) Gross, D. S.; Rodriguez-Cruz, S. E.; Bock, S.; Williams, E. R. *J. Phys. Chem.* **1995**, *99*, 9,4034.
(47) Williams, E. R. *J. Mass Spectrom.* **1996**, *31*, 831.
(48) Hettich, R. L.; Compton, R. N.; Rotchie, R. H. *Phys. Rev. Lett.* **1991**, *67*, 1242.
(49) Limbach, P. A.; Schweikhard, L.; Cowen, K. A.; McDermott, M. T.; Marshall, A. G.; Coe, J. V. *J. Am. Chem. Soc.* **1991**, *113*, 6795.
(50) Wang, X. B.; Ding, C. F.; Wang, L. S. *J. Chem. Phys.* **1999**, *110*, 8217.

The ordering of the d-orbitals was controversial in the early studies, but it is now fairly well understood. The ordering of the d-orbitals shown in Figure 4 is basically accepted currently, i.e., the highest occupied MO (HOMO) of $PtCl_4^{2-}$ is the $2b_{2g}$ (d_{xy}) orbital, followed by the degenerate $2e_g$ (d_{xz}, d_{yz}) and the $3a_{1g}$ (d_{z^2}) MO's. However, the ordering of the ligand-derived MO's and their separations relative to the d-orbitals are much less well understood. The latest theoretical study on the electronic structure of $PtCl_4^{2-}$ was done by Larsson, Olsson, and Rosen (LOR),[18] who performed both nonrelativistic and relativistic calculations using extended-Huckel and discrete variational methods. Since the extended-Huckel method gave the wrong ordering for the d-orbitals, we will use the results from their discrete variational method to interpret our PES spectra. The ordering of the occupied MO's from the nonrelativistic calculations by LOR is as follows: $2b_{2g} > 2e_g > 3a_{1g} > 1a_{2g} > 3e_u > 1b_{2u} > 1a_{2u} > 2e_u > 1e_g > 1b_{2g} > 2a_{1g} > 2b_{1g}$. We will show that this MO ordering is basically consistent with our observed PES spectra of $PtCl_4^{2-}$. The spectra of $PtBr_4^{2-}$ can also be interpreted using this MO picture. However, we found that the first ligand-derived MO, $1a_{2g}$, is above the last d-orbital, $3a_{1g}$ (d_{z^2}), in $PtBr_4^{2-}$.

The X, A, and B Features. The first three low binding energy features X, A, and B of $PtCl_4^{2-}$ (Figure 1) are almost identical with those of $PtBr_4^{2-}$ (Figure 2), except that they are slightly shifted to the high BE side in the bromide complex. Their spacings are essentially the same in the two complexes within our experimental uncertainty, as indicated in Table 1 (ΔE, relative to the X feature). The relative intensities of the three features in the spectra of both complexes are also roughly the same at the different photon energies. These three features should be due to detachment from MO's mainly of 5d characters. The X feature is assigned from removal of an electron from the HOMO, $2b_{2g}$ (d_{xy}). The next MO is the degenerate $2e_g$ (d_{xz}, d_{yz}), which should give rise to two detachment features due to spin−orbit or Jahn−Teller effects. Thus we attribute the A and B features to the $2e_g$ MO. Note that we are using the MO symbols derived from the nonrelativistic calculations for simplicity. As shown by LOR, when relativistic effects are "switched on", the degeneracy of the $2e_g$ MO is lifted and will be split into two nondegenerate MO's.[18] Therefore, the splitting upon detachment of a $2e_g$ electron is more appropriately viewed as due to the spin−orbit splitting, rather than the Jahn−Teller effect. The nearly identical spacings among the X, A, and B features in the Cl and Br complexes suggest that the ligand contributions to the $2b_{2g}$ and $2e_g$ MO's are rather small.

The C and D Features. The next MO is $3a_{1g}$ due to the d_{z^2}-orbital, followed by the first ligand-based MO, $1a_{2g}$. The C and D features should be due to detachment from these two orbitals. However, the relative intensity changes of the C and D features between the 193- and 266-nm spectra are exactly opposite in the two complexes. In the $PtCl_4^{2-}$ spectra, the C feature was very intense at 193 nm, but decreased at 266 nm, whereas in the $PtBr_4^{2-}$ spectra the D feature showed this behavior. We think that this subtle spectral difference in the two complexes suggests that the C and D features are from different MO's in the two complexes. We thus assigned the C and D features to be from the $3a_{1g}$ and $1a_{2g}$ MO's, respectively, in $PtCl_4^{2-}$. In $PtBr_4^{2-}$, we assigned the C feature as being from $1a_{2g}$ and the D feature from $3a_{1g}$. These assignments are supported by two observations. First, these assignments yielded identical spacings among the four d-orbitals in the two complexes, as expected (see Table 1). Second, because Br^- has a smaller electron binding energy than Cl^-, the ligand-derived $1a_{2g}$ MO is expected to have a smaller BE in the bromide complex as well. Although there has been no previous calculation on the electronic structure of $PtBr_4^{2-}$, the current observation of the change of relative ordering between the 5d- and ligand-derived MO's in the two complexes is rather conclusive and would be interesting to confirm by further theoretical studies.

The E and F Features. The E and F features have different relative spacing in the two complexes, but they showed similar photon-energy dependence from 193 to 266 nm. The relative spacing in the Br complex is nearly twice as large as that in the Cl complex (Table 1). According to the MO ordering by LOR, the next MO should be the ligand-derived $3e_u$-orbital, which is expected to result in two detachment features due to the spin−orbit splitting, as shown above for the $2e_g$ MO. Thus the E and F features are assigned to be from detachment of a $3e_u$ electron. The increased spacing between the two features in the Br complex is exactly what one would expect because of the large spin−orbit effect in Br compared to that in Cl. The change of spacing between the Cl and Br complexes provides rather firm evidence for the assignment of the E and F features to the $3e_u$ MO. Such change of spacing is a good signature to identify ligand-based MO's and has been used very effectively in our previous investigation of hexahalogenometalate doubly charged metal complexes for such purposes.[30]

The G, H, and I Features. These high BE features exhibited similar relative spacings in the two complexes, except that the intensities of the H and I features were rather low in the spectrum of the Br complex (Figure 2a). According to the MO ordering by LOR, the G and H features can be assigned straightforwardly to the $1b_{2u}$ and $1a_{2u}$ ligand-derived MO's, respectively. However, the assignment of the I feature is less straightforward. According to the MO ordering of LOR, the next MO is the ligand-based $2e_u$-orbital. This is a degenerate MO and two features were expected from detachment from this MO, as shown above for the $2e_g$ and $3e_u$ MO's. If the splitting were similar to that for the E and F features ($3e_u$), we would have expected to observe the second component because the 193-nm photon would be still above the RCB for this state. If the splitting were much larger, the second component may have too high a binding energy for it to be observed due to the RCB. It is interesting that the relativistic calculations by LOR for $PtCl_4^{2-}$ did give a significantly larger splitting for the $2e_u$ MO compared to that of $3e_u$.[18] Thus it is possible that the expected second component eluded our observation due to its high binding energy. We tentatively assigned the I feature to be from the $2e_u$ MO.

MO Orderings and Correlation Diagram between $PtCl_4^{2-}$ and $PtBr_4^{2-}$. Figure 5 shows the MO ordering that we observed in conjunction with the theoretical calculations by LOR. Vertical binding energies from Table 1 were used in the figure, where for the degenerate MO's the average of the two observed components was used. As discussed above, the MO ordering obtained by LOR in their nonrelativistic calculations for $PtCl_4^{2-}$ seems to be qualitatively consistent with our data. However, for quantitative comparison, relativistic calculations would be required due to the strong relativistic effects anticipated for Pt. We note that the relativistic calculations by LOR did not provide a quantitative picture to compare with our data, which is probably not surprising. We emphasize that the current data provide the most detailed electronic structure information available for these classical D_{4h} metal complexes and would be

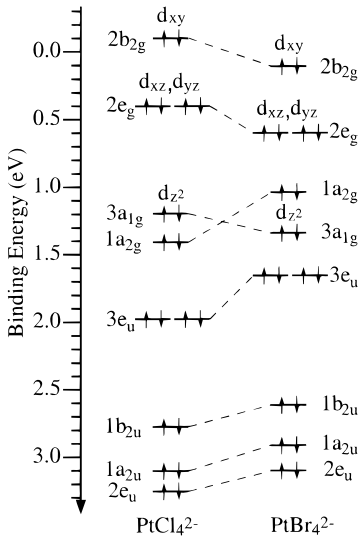

Figure 5. Schematic diagram summarizing the molecular orbital energy levels obtained from the current study and the correlation between $PtCl_4^{2-}$ and $PtBr_4^{2-}$.

valuable to compare to or confirm any future more accurate relativistic ab initio calculations.

Figure 5 also shows clearly that the MO's derived mainly from the d-orbitals are all above the ligand-based MO's in $PtCl_4^{2-}$. From $PtCl_4^{2-}$ to $PtBr_4^{2-}$, all the d-orbitals are seen to be stabilized. This is mainly an electrostatic effect because the Pt−Br bonds are longer and the Br complex has a larger size, consequently a smaller intramolecular electrostatic repulsion. The ligand-based orbitals, on the other hand, are all destabilized in the Br complex, mainly due to the low electron affinity of Br relative to Cl. Thus the opposite trends of the d- and ligand-orbitals from the Cl to the Br complex led to the overlap between the d- and ligand-orbitals in $PtBr_4^{2-}$.

Conclusions

We have observed two pentaatomic doubly charged anions, PtX_4^{2-} (X = Cl, Br), in the gas phase. These free dianions were found to be metastable against electron autodetachment, with a negative electron binding energy of −0.25 and −0.04 eV for the chloride and bromide complexes, respectively. The photon-energy-dependent PES spectra clearly revealed the dianion nature of these species and allow the RCB to be estimated. The net Coulomb repulsion energy in $PtBr_4^{2-}$ (∼2.1 eV) is smaller than that in $PtCl_4^{2-}$ (∼2.5 eV), which is consistent with the slightly larger size and long lifetime for the bromide complex. These two species are among the smallest dianions that have been observed in the gas phase.[31]

Well-resolved detachment features were obtained in the PES spectra for the two species, yielding a wealth of electronic structure information about both the dianions and the singly charged species. Detachment from metal d-orbitals or ligand-orbitals was observed and could be clearly distinguished. In $PtCl_4^{2-}$, all the d-orbitals are found to be above the ligand-orbitals. In $PtBr_4^{2-}$, the d-orbitals are stabilized while the ligand-orbitals are destabilized, leading to an overlap between the d- and ligand-orbitals, i.e., the first ligand-orbital is found to be above the last d-orbital. Although the current data were qualitatively interpreted using currently available theoretical calculations, the unprecedented well-resolved spectral features from this gas-phase study will be valuable to verify more accurate calculations for these classical and prototypical square-planar transition metal complexes.

Acknowledgment. This work was supported by the National science Foundation (CHM-9817811). Acknowledgment is also made to the donors of the Petroleum Research Fund, administered by the American Chemical Society, for partial support of this research. This work was performed at the W. R. Wiley Environmental Molecular Sciences Laboratory, a national scientific user facility sponsored by Department of Energy's Office of Biological and Environmental Research and located at Pacific Northwest National Laboratory. Pacific Northwest National laboratory is operated for the U.S. Department of Energy by Battelle. L.S.W. is an Alfred P. Sloan Foundation Research Fellow.

JA9935106